Original Article
Role of ferroptosis-related molecular patterns in hepatocellular carcinoma microenvironment

Jukun Wang, Yu Li, Chao Zhang, Xin Chen, Linzhong Zhu, Tao Luo

Department of General Surgery, Xuanwu Hospital, Capital Medical University, Beijing, China

Abstract: Heterogeneity and complexity of hepatocellular carcinoma (HCC) have been an impediment to effective diagnosis and treatment of HCC. Mounting evidence suggests that ferroptosis-related genes (FRGs) regulate the development of HCC by affecting the tumor microenvironment (TME). Herein, we explored the role of ferroptosis-related molecular patterns in the HCC microenvironment. The transcriptome and corresponding clinicopathological data of HCC patients were downloaded from The Cancer Genome Atlas (TCGA) and the Gene Expression Omnibus (GEO) database, respectively. Molecular patterns of ferroptosis were explored using consensus clustering analysis and ferroptosis-related molecular patterns in the individual patients were analyzed using principal component analysis (PCA). The ability of ferroptosis-related patterns to predict the biological status and survival outcomes of HCC patients was investigated. Based on the expression of FRGs, three molecular patterns related to ferroptosis were identified. Single sample gene set enrichment analysis (ssGSEA) showed that the molecular patterns associated with the worst prognosis were significantly correlated with high infiltration of immunosuppressive cells in the TME. Besides, we identified three ferroptosis gene clusters underlying the different biological features of the three ferroptosis patterns. Patients in the high-risk group had a worse biological status and survival outcomes than those in the low-risk group. This study demonstrates that ferroptosis-related molecular patterns lead to high heterogeneity in HCC. These molecular patterns can be used to assess the survival of HCC patients and guide the design of immunotherapy strategies for HCC patients.

Keywords: Hepatocellular carcinoma, TCGA, ferroptosis, prognosis

Introduction

Liver cancer is the sixth most prevalent and fourth leading cause of mortality [1]. Hepatocellular carcinoma (HCC) is the most common type of liver cancer, accounting for 75-85% of all primary liver cancers [2]. HCC is mainly caused by a hepatitis virus infection, aflatoxin, heavy alcohol consumption, and type 2 diabetes [3, 4]. However, due to its insidious onset and rapid progression, most HCC patients are diagnosed at an advanced stage, making them unfit for surgical therapy [5]. Moreover, its complex tumor microenvironment (TME) causes biological heterogeneity, creating difficulty in the management of patients. Therefore, precise diagnosis and treatment of HCC depend on a comprehensive understanding of TME complexity and heterogeneity.

Ferroptosis, a newly discovered type of programmed cell death, differs from autophagy, apoptosis, and necrosis, and is characterized by iron-dependent lipid peroxide accumulation [6, 7]. Ferroptosis has been implicated in multiple tumors, including HCC [8]. Redox state imbalance, an important event during the occurrence and development of tumors, is often accompanied by high demand for iron ions, suggesting that tumor cells are susceptible to ferroptosis [9]. Sun et al. reported that inhibition of metallothionein-1G expression enhanced anticancer effects of sorafenib by inducing ferroptosis in HCC cells [10]. Liang et al. constructed a prediction model using ferroptosis-related genes (FRGs) and demonstrated that ferroptosis-related risk signature can predict survival of HCC patients and relative proportion of tumor-associated cell infiltration in the HCC microenvironment [11]. Elsewhere, CD8+ T cells in the TME were found to induce ferroptosis of tumor cells through secreting IFNγ which inhibited the expression of SLC3A2

and SLC7A11 [12]. Overall, these studies demonstrated that ferroptosis influence the TME.

In this study, we first identified three molecular patterns related to ferroptosis using consensus clustering analysis. Three molecular patterns associated with the survival and immune cell infiltration were identified. Furthermore, we identified three distinct ferroptosis gene clusters that were responsible for the biological differences among the three molecular patterns and calculated ferroptosis score for each patient based on distinct molecular patterns. This study provides reference data for improving the treatment of HCC patients.

Material and methods

Data processing

The transcriptome, somatic mutation, and corresponding clinicopathological data of 371 HCC patients were obtained from The Cancer Genome Atlas (TCGA) (https://portal.gdc.cancer.gov/). Fragments per kilobase million (FPKM) values were transformed into transcripts per kilobase million (TPM). Data of 225 samples were retrieved from the Gene Expression Omnibus (GEO) database (GSE14520) (https://www.ncbi.nlm.nih.gov/geo/) and were combined with samples from TCGA cohort. The copy number variation (CNV) data were downloaded from the University of California Santa Cruz (UCSC) genome browser (https://xena.ucsc.edu/). A total of 60 FRGs were obtained from previous literature. The study was conducted in accordance with the Declaration of Helsinki (as revised in 2013).

Identification of differentially expressed FRGs

Differentially expressed FRGs between HCC and adjacent normal tissues were identified using R package 'limma' and the Wilcoxon test. The somatic mutation and CNV of FRGs were analyzed with the R software.

Ferroptosis-based consensus clustering analysis

Samples from the TCGA and GEO datasets were merged after correcting differences between batches. Consensus clustering analysis was conducted to determine the number of ferroptosis-related molecular patterns based on the expression of FRGs using the R package 'ConsensusClusterPlus'. To compare the sur-vival time between molecular patterns, Kaplan-Meier survival analysis was performed using R packages 'survival' and 'survminer', followed by log-rank test. The distribution of molecular patterns was estimated using Principal component analysis (PCA). R package 'GSVA' was utilized to quantify the infiltration level of immune cells based on ssGSEA algorithm. The Kruskal-Wallis test was performed to compare differences among different groups.

Analysis of ferroptosis gene clusters

A Venn diagram was constructed using the R package 'VennDiagram' for identification of common differentially expressed genes (DEGs) (adjusted P<0.001). The common DEGs related to the overall survival (OS) of HCC patients were further selected using univariate Cox regression analysis (P<0.05). Next, consensus clustering analysis was conducted to determine the number of ferroptosis gene clusters responsible for biological differences between molecular patterns based on the expression of independent prognostic DEGs. Differences in survival between ferroptosis gene clusters were estimated using Kaplan-Meier analysis. The ferroptosis gene clusters were verified using PCA analysis.

Quantification of ferroptosis score using PCA analysis

Based on independent prognostic DEGs, we developed a ferroptosis scoring system to quantify the ferroptosis-related molecular pattern of each patient according to ferroptosis gene clusters using PCA analysis via R function 'prcomo'. We used PC1 and PC2 as the signature scores of ferroptosis patterns based on previous studies [13]. The ferroptosis score for each patient was calculated as follows:

Ferroptosis Score = $\sum (PC1i + PC2i)$

Where i represents the expression of independent prognostic DEGs. Kaplan-Meier analysis was used to determine the optimum cut-off value of ferroptosis scores. Then, we divided all patients into high- and low-risk groups based on the ferroptosis score.

Sankey plot was generated to show the distribution of both the ferroptosis score and survival status for each patient using the R package 'ggalluvial'. Survival differences between the high- and low-risk groups were compared using
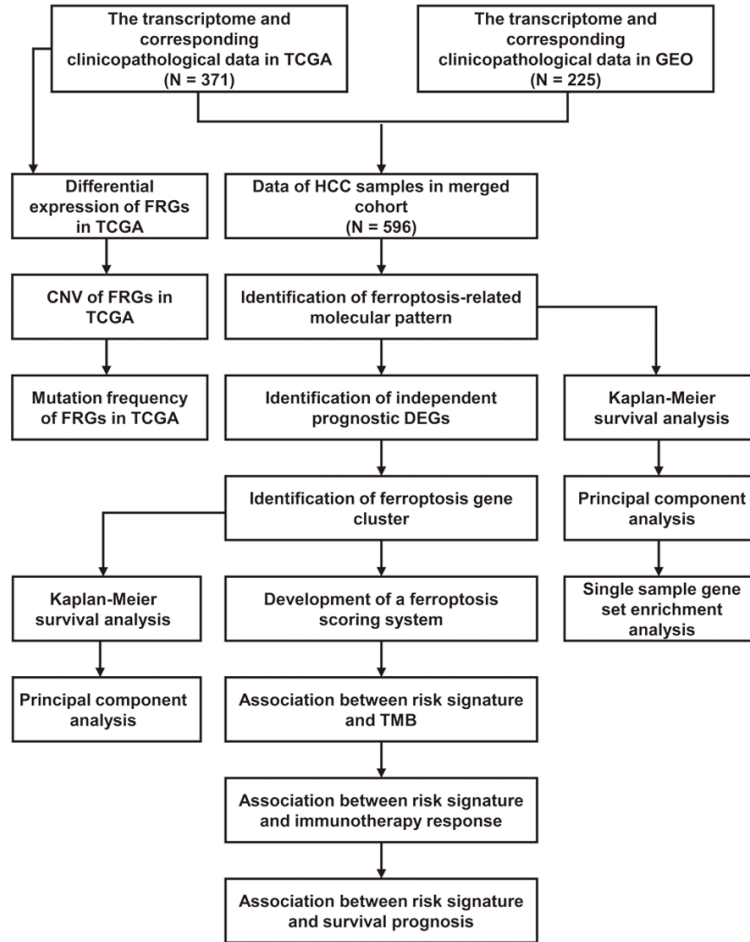
Figure 1. The workflow of data collection and analysis process.

Kaplan-Meier analysis, followed by log-rank test. Besides, the differences in the distribution of ferroptosis scores among ferroptosis-related molecular patterns or gene clusters were analyzed using Kruskal-Wallis test.

Evaluation of differences in tumor mutation burden (TMB) or immunotherapy response in the high- and low-risk groups

The visualization of the Mutation Annotation Format (MAF) files was conducted using package 'Maftools' in R. The difference in the expression of immune checkpoint molecules, including programmed cell death protein 1 (PD-1) and cytotoxic T-lymphocyte-associated protein 4 (CTLA-4), between high- and low-risk groups was revealed using Wilcoxon test. The Cancer Immunome Atlas (TCIA) database (https://tcia.at/home) was used to validate immunotherapy score results in HCC patients from the TCGA cohort. R package 'ggpubr' was utilized to calculate the difference in the immu-

notherapy score between different groups.

Estimation of the predictive ability of the ferroptosis scoring system for patients with clinicopathological features

The information of patients with clinicopathological features was retrieved from the TCGA database. Wilcoxon test was utilized to analyze the difference in the distribution of ferroptosis score between subgroups under the same clinicopathological feature (including Age >65 vs. Age ≤65, Male vs. Female, and Stage I-II vs. Stage III-IV). Besides, Kaplan-Meier analysis and log-rank test were used to compare survival differences in each subgroup (including Age >65, Age ≤65, Male, Female, Stage I-II, and Stage III-IV).

Statistical analysis

All statistical analyses were performed using R software (version 4.0.2). Wilcoxon test was used to compare differences between the two groups. Kruskal-Wallis test was utilized to analyze differences among three or more groups. Kaplan-Meier method was used to generate survival curves for OS in different groups. Differences in survival time between groups were estimated using the log-rank test. Univariate Cox regression analysis was utilized to estimate independent prognostic DEGs for OS in HCC patients. *P*-values less than 0.05 (*P*<0.05) were considered statistically significant.

Results

FRGs landscape in HCC

Figure 1 shows a workflow of data collection and analysis process. Most of FRGs were differentially expressed between HCC and adjacent normal tissues (**Figure 2A**). Further analysis showed that copy number gain was more common than copy number loss (**Figure 2B**). Among the three FRGs, TP53 had the highest

Ferroptosis-related molecular patterns
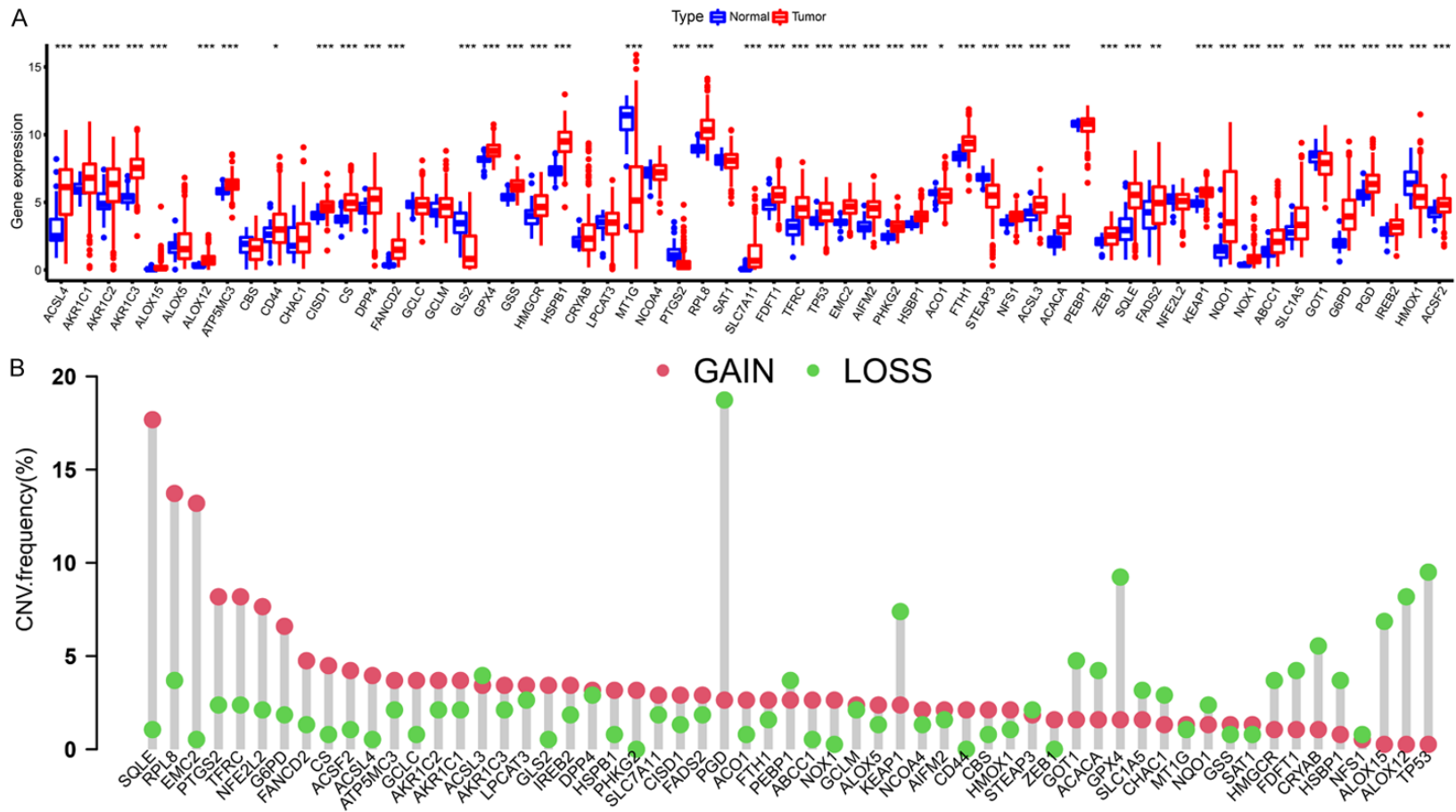
Figure 2. Expression of ferroptosis-related genes (FRGs) in HCC. A. Differential expression of FRGs in HCC and adjacent normal tissues. B. Copy number variation of FRGs in HCC patients from TCGA cohort. Asterisks represent levels of significance *P<0.05, **P<0.01, ***P<0.001.

Ferroptosis-related molecular patterns
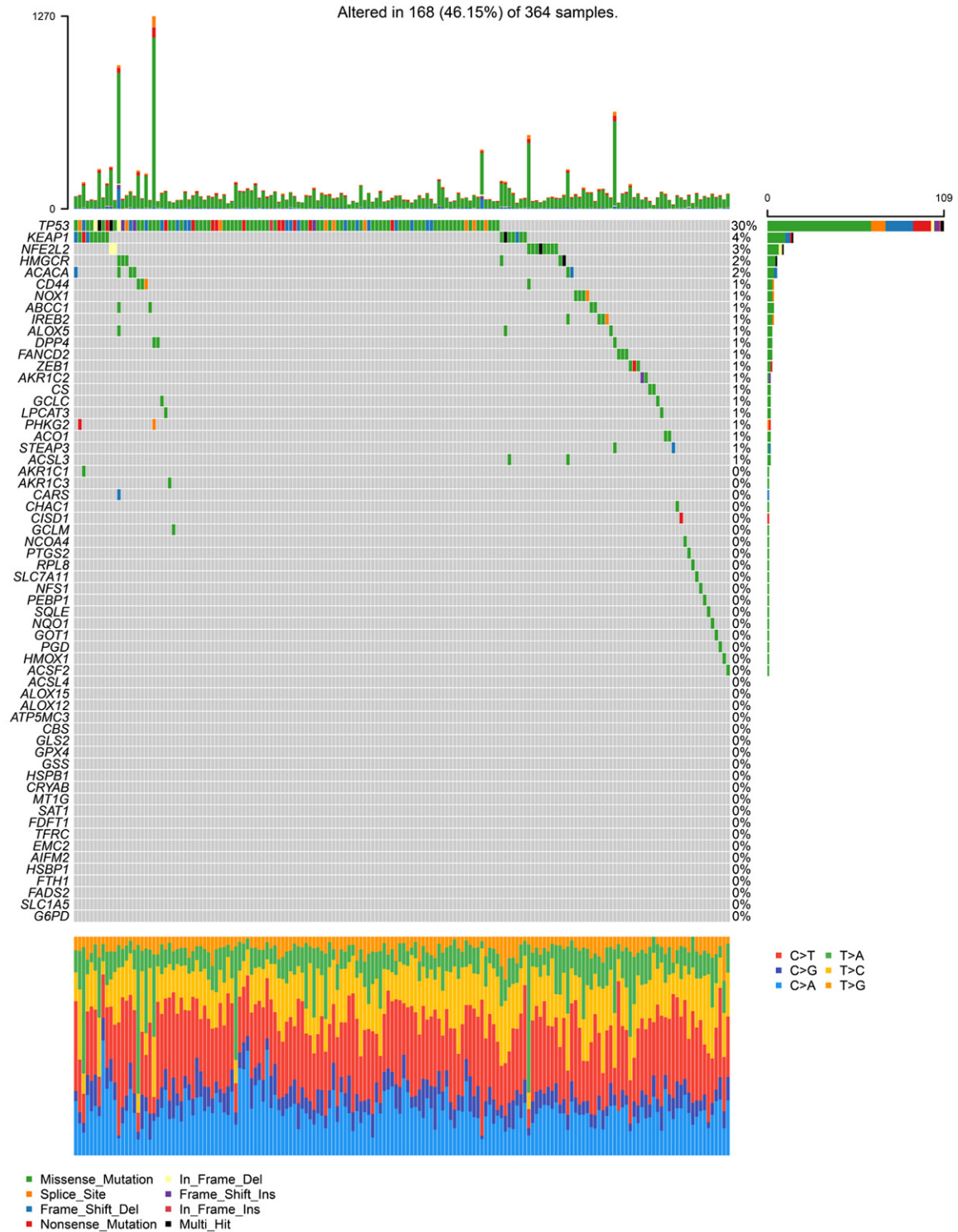
Figure 3. Mutation frequency of FRGs in HCC patients from TCGA cohort. TP53 had the highest mutation frequency (30%), followed by KEAP1 (4%), and NFE2L2 (3%), indicating that the mutation frequency of FRGs is relatively low in HCC.

mutation frequency (30%), followed by KEAP1 (4%), and NFE2L2 (3%), indicating that the mutation frequency of FRGs was relatively low (**Figure 3**).

Identification of ferroptosis-related molecular patterns

A total of 596 HCC patients were merged, including 371 patients from TCGA and 225 patients from GSE14520. Subsequently, the expression profile of FRGs was extracted from the merged dataset for consensus clustering analysis. The cumulative distribution function (CDF) curve and the area under the CDF curve indicated that 3 was temporarily selected as the appropriate k-value (**Figure 4A**, **4B**). The correlation within each subgroup was strong whereas that between each subgroup was weak (**Figure 4C**). Moreover, the samples within each subgroup were evenly distributed (**Figure 4C**). Therefore, we divided all samples into three ferroptosis-related molecular patterns (A, B, and C).

Analysis of differences in the survival prognosis and immune cells infiltration between ferroptosis-related molecular patterns

Figure 4D indicated that patients in molecular pattern C had the worst prognosis (P<0.001). PCA analysis showed that the three patterns were distinct (**Figure 4E**). Moreover, the heatmap showed a correlation between the three patterns and clinicopathological features (**Figure 4F**). Besides, ssGSEA revealed significant differences in the infiltration levels of immune cells among the three patterns, especially tumor-associated macrophages (TAMs), regulatory T cells (Tregs), and myeloid-derived suppressor cells (MDSCs) (**Figure 4G**).

Identification of common DEGs among the three molecular patterns

Figure 5 showed that a total of 261 common DEGs were identified (adjusted P<0.001). After univariate Cox regression analysis for OS, 236 genes with potential independent prognostic value were selected for further analysis.

Identification and analysis of ferroptosis gene clusters

According to the expression of the 236 genes, the number of ferroptosis gene clusters was determined using consensus clustering analysis. Based on the CDF curve and the area under the CDF curve, 3 was temporarily selected as the appropriate k-value (**Figure 6A**, **6B**). The correlation within each subgroup was strong

whereas that between each subgroup was weak (**Figure 6C**). In addition, the samples within each subgroup were evenly distributed (**Figure 6C**). Therefore, we divided all patients into three ferroptosis gene clusters (D, E, and F).

Figure 6D showed that patients in gene cluster F had the worst prognosis. PCA analysis revealed that patients can be divided into three different regions (**Figure 6E**). Similarly, the heatmap showed an association between the three gene clusters and clinicopathological features (**Figure 6F**). **Figure 6G** indicated that most of the FRGs were differentially expressed among all ferroptosis gene clusters.

Construction and assessment of the ferroptosis scoring system

We divided all patients into high- (n=60) and low-risk (n=531) groups based on the optimum cut-off value of the ferroptosis score. Sankey diagram showed the distribution changes of both ferroptosis molecular patterns and ferroptosis gene clusters (**Figure 7A**). Patients in molecular pattern C had significantly higher ferroptosis scores compared to those in molecular pattern A or B (**Figure 7B**). Meanwhile, patients in gene cluster F had significantly higher ferroptosis score compared with those in gene clusters D or E (**Figure 7C**). Results shown in **Figure 7D** indicated that patients in the high-risk group had worse prognosis than those in the low-risk group, confirming our previous findings.

Correlation between ferroptosis score and TMB

Compared with patients with low TMB, patients with high TMB had worse survival outcomes (**Figure 8A**). Further, among patients with low TMB, those with a low ferroptosis score had better survival outcomes than those with a high ferroptosis score (**Figure 8B**). Besides, TP53 mutation frequency was higher in the high-risk group than in the low-risk group (**Figure 8C**, **8D**).

Association of ferroptosis score with response to immunotherapy

The expression levels of PD-1 and CTLA-4 showed significant differences between high- and low-risk groups (**Figure 9A**, **9B**). Additional-
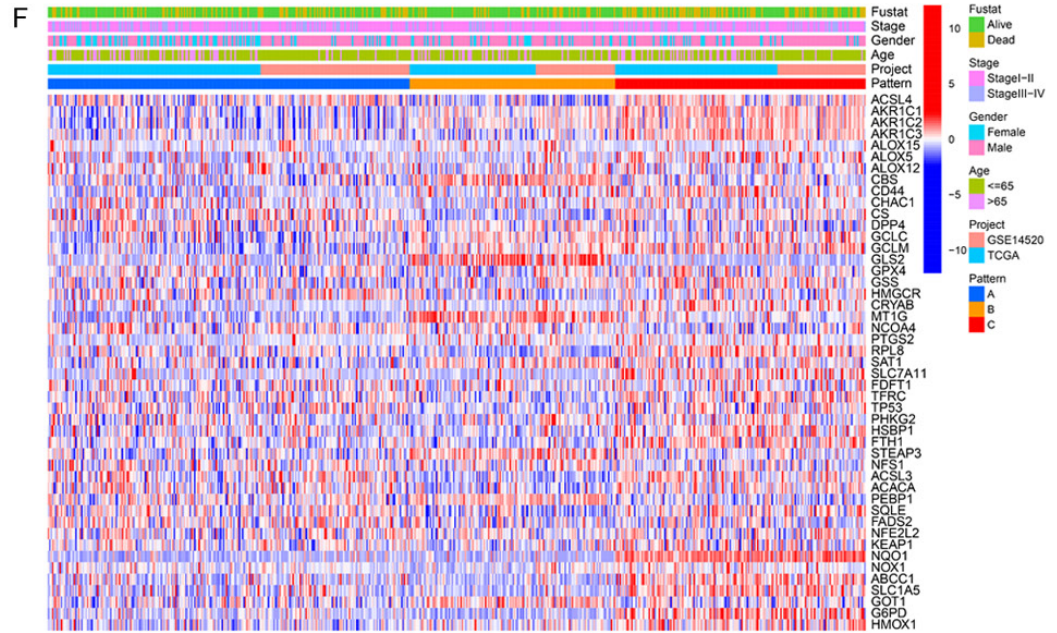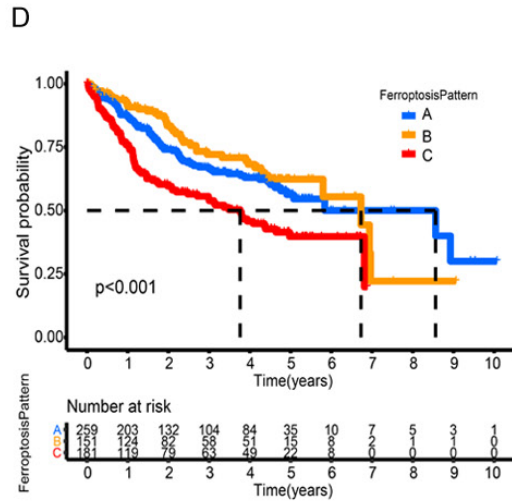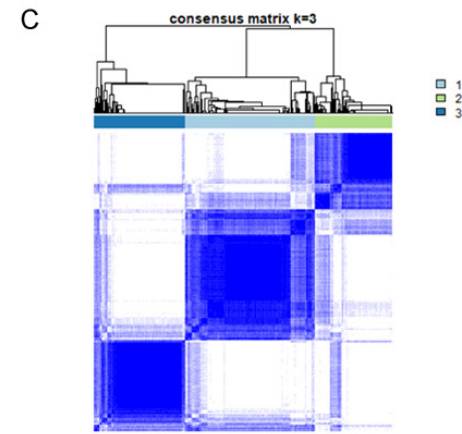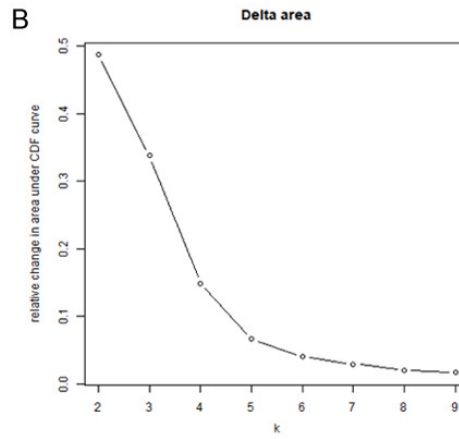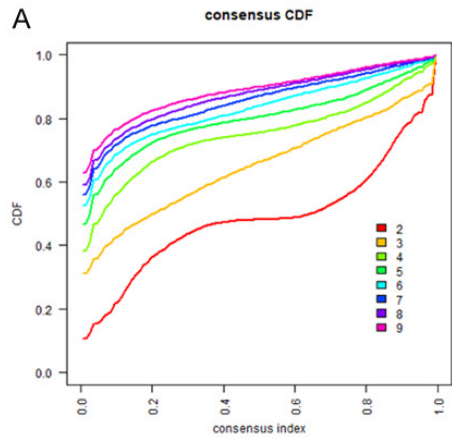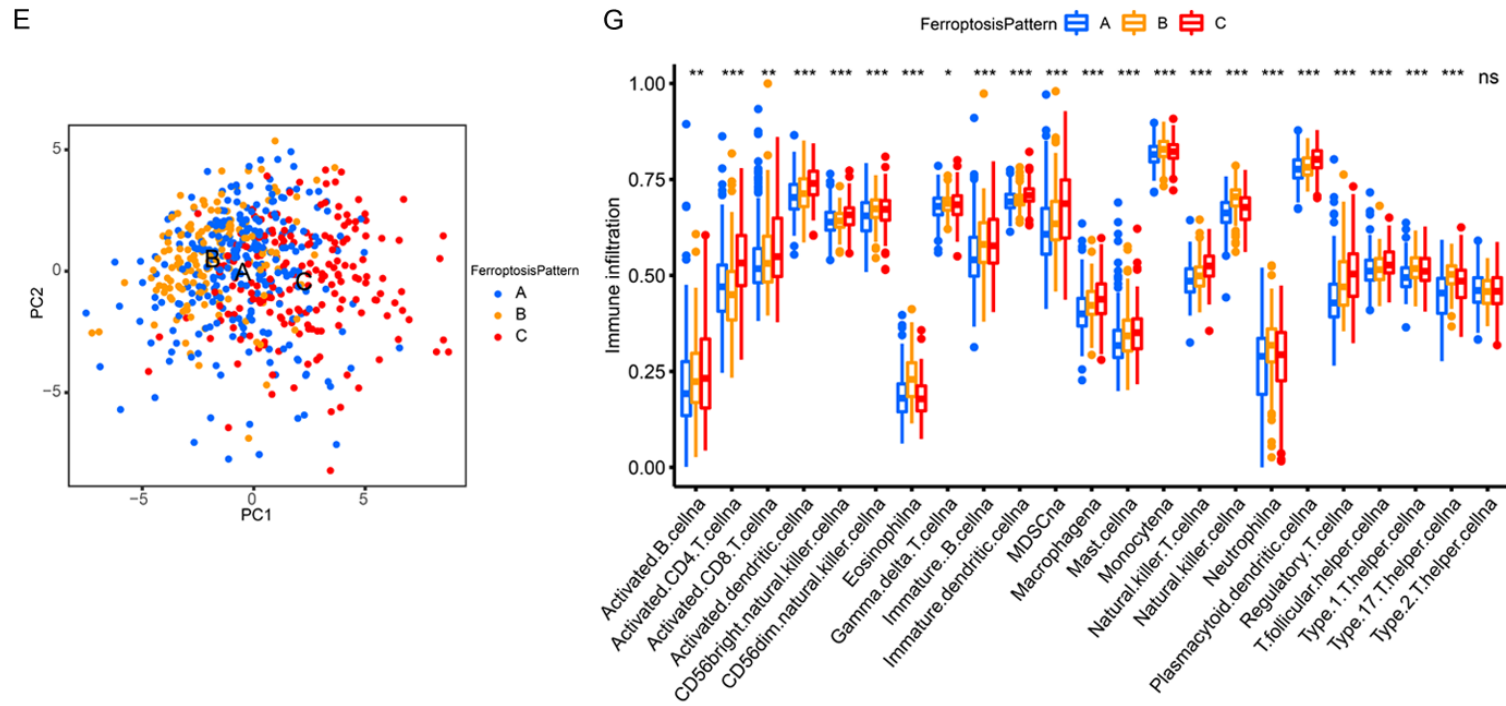
Figure 4. Identification and analysis of ferroptosis-related molecular patterns based on expression of FRGs. A. The distribution of cumulative distribution function (CDF) curves. B. The area under the CDF curve. C. Heatmap of clusters of merged cohorts when k=3. D. Kaplan-Meier survival curves depicting the survival outcomes of the three ferroptosis-related molecular patterns. E. Principal component analysis (PCA) for distribution of the three ferroptosis-related molecular patterns. F. Heatmap showing the correlation between ferroptosis-related molecular patterns and clinicopathological features. G. Differences in the infiltration levels of immune cells among the three ferroptosis-related molecular patterns.
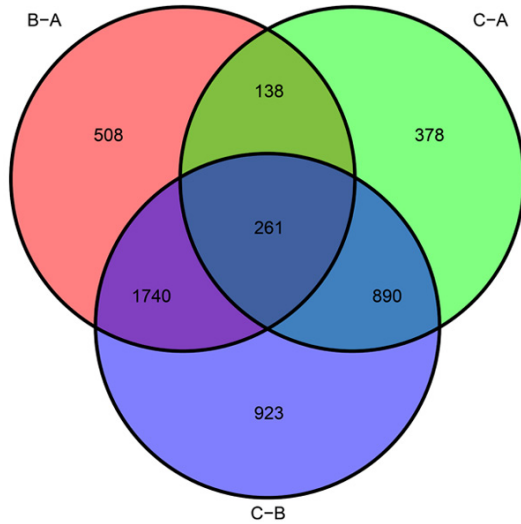
Figure 5. Venn plot showing common DEGs among the three ferroptosis-related molecular patterns.

ly, patients in the low-risk group had better immunotherapy response compared to those in the high-risk group, including anti-PD-1 monotherapy, anti-CTLA-4 monotherapy, and a combination of anti-PD-1 and anti-CTLA-4 (**Figure 9C-F**). These findings suggest that ferroptosis score could assess response to anti-PD-1 and anti-CTLA-4 immunotherapy.

Prognostic value of ferroptosis score in HCC patients

We found significant differences in the distribution of ferroptosis score between subgroups of both age (Age >65 vs. Age ≤65) and stage (Stage I-II vs. Stage III-IV) (**Figure 10A-C**). Besides, Kaplan-Meier survival analysis indicated that the ferroptosis score had a better predictive ability in survival outcomes of HCC subgroup patients (including Age >65, Age ≤65, Male, Female, Stage I-II, and Stage III-IV) (**Figure 10D-I**). Therefore, the ferroptosis score was expected to be a predictor of prognosis in patients with HCC.

Discussion

Although significant progress has been achieved in the treatment of HCC, the survival of HCC patients remains poor. Moreover, the currently used TNM staging system does not fully reflect the biological heterogeneity of HCC; therefore it is not effective for diagnosis and treatment of HCC. Molecular patterns based on

molecular pathology can reflect deeper characteristics of tumors and therefore compensate for the deficiencies of the TNM staging system.

Since the discovery of ferroptosis, numerous studies have found that ferroptosis plays a role in the occurrence and progression of HCC. Moreover, abnormal iron absorption and lipid metabolism disorders, two key factors that regulate ferroptosis, have been observed in patients with HCC [14-16]. In the present study, we identified three ferroptosis-related molecular patterns based on the expression of FRGs. Then, we developed a ferroptosis scoring system for each patient to predict the survival of patients and TME characteristics.

The expression of FRGs was higher in HCC tissues than in adjacent normal tissues. Besides, CNVs of FRGs were common while mutation frequencies were very low. These findings are consistent with those of a previous study on 24 FRGs in 20 cancers, including HCC [17]. Our results also confirmed that copy number gain of FRGs was positively correlated with increased expression of FRGs in HCC. Liu et al. found that the expression levels of most FRGs were significantly associated with CNV in HCC [17].

Based on the expression of FRGs, we identified three ferroptosis-related molecular patterns using consensus clustering analysis. Kaplan-Meier survival analysis indicated that most FRGs were upregulated in molecular pattern C, which was associated with the worst survival prognosis. Liang et al. found that expression levels of 26 FRGs in HCC tissues were higher than those in adjacent normal tissues, and these upregulated genes were risk factors for poor prognosis of HCC patients [11]. Interestingly, NQO1 was increased in HCC tissues, and its level was higher in molecular pattern C than in corresponding molecular pattern A or B, which was analogous with a previous finding that overexpression of NQO1 enhanced the proliferation of HCC cells via SIRT6/AKT/XIAP signaling pathway [18]. Yang et al. reported that patients with high NQO1 levels had a poor survival prognosis and that NQO1 can promote the growth and aggressiveness of HCC [19]. These results further suggested that FRGs may be potential biomarkers for prognostic prediction and targeted treatment of HCC.
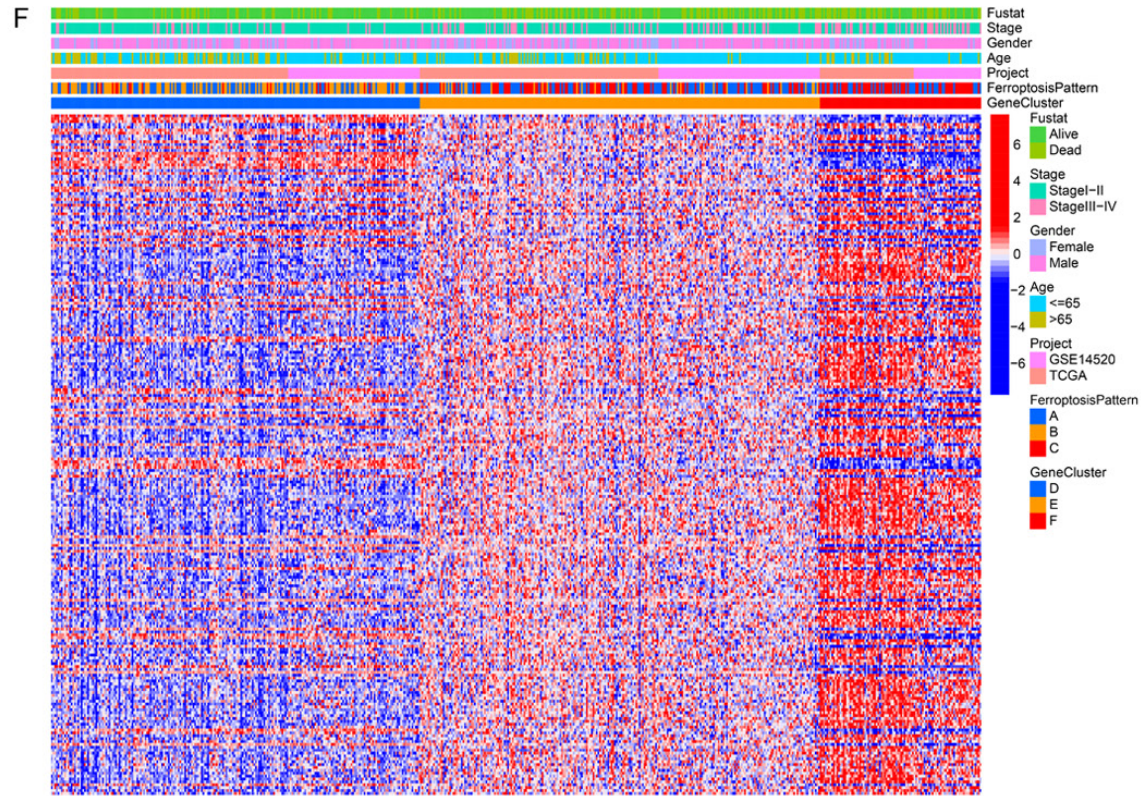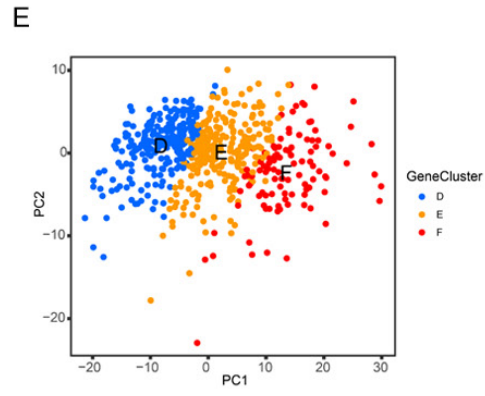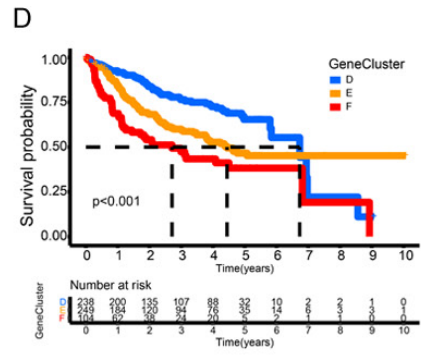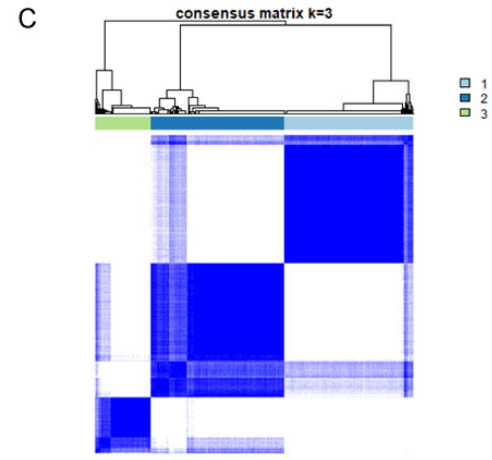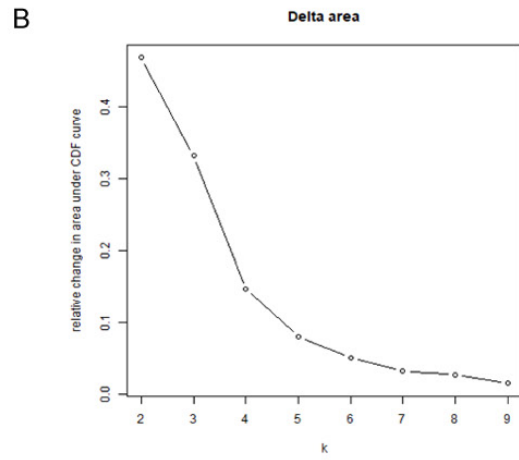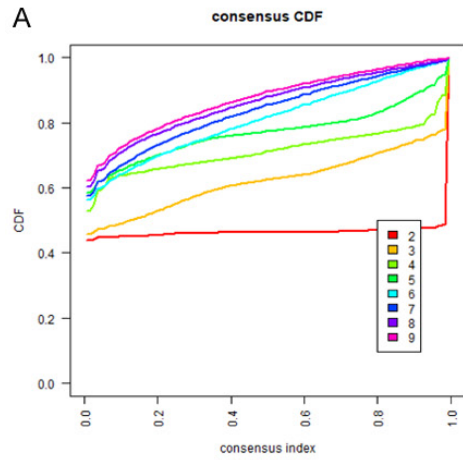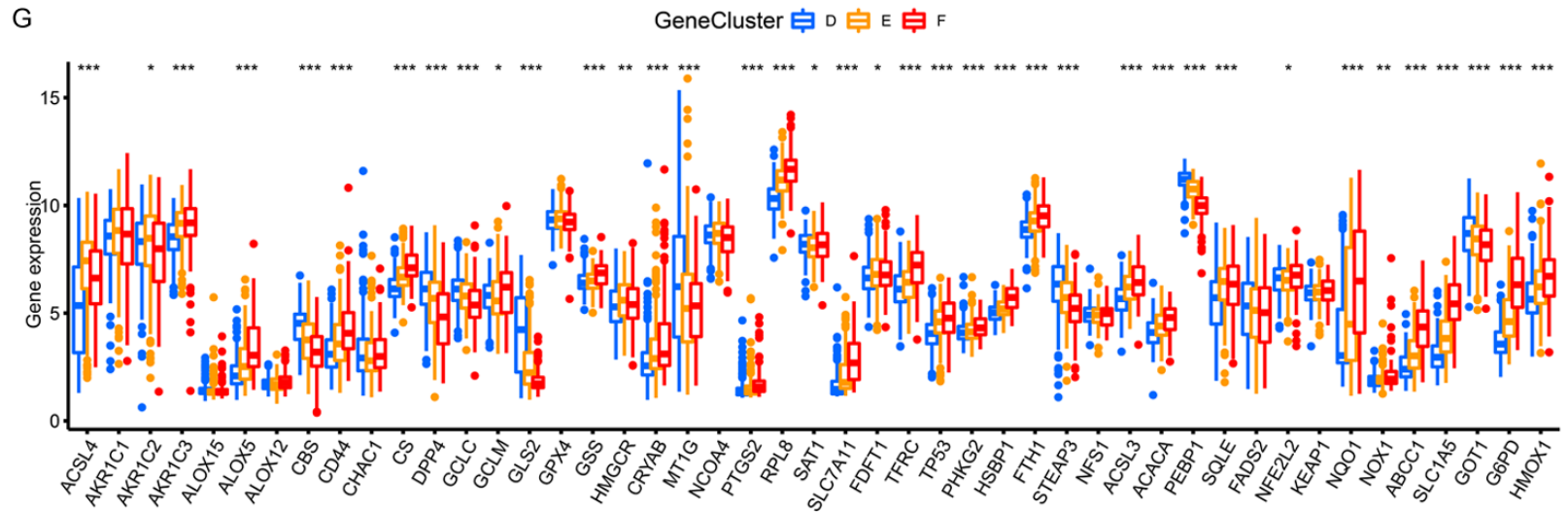
Figure 6. Identification and analysis of ferroptosis gene clusters based on the expression of common DEGs. A. The distribution of cumulative distribution function (CDF) curves. B. Area under the CDF curve. C. Heatmap of merged cohort clusters when k=3. D. Kaplan-Meier survival analysis of the three ferroptosis gene clusters. E. PCA estimating the distribution of the three ferroptosis-related molecular patterns. F. Heatmap showing correlation between the three ferroptosis gene clusters and clinicopathological features. G. Differences in the distribution of FRGs in ferroptosis-related gene clusters.
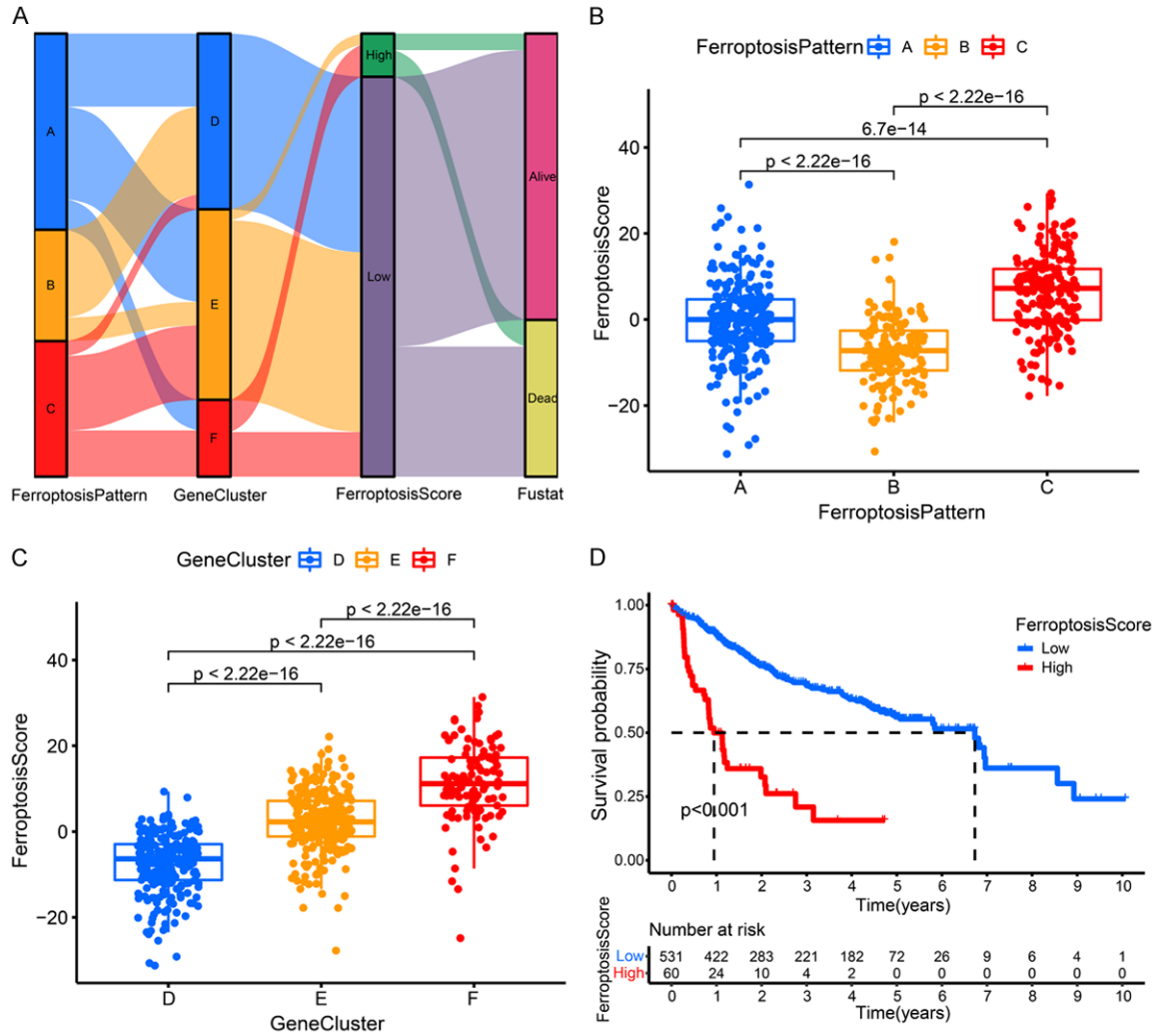
Figure 7. Distribution of ferroptosis scores for HCC patients. A. Sankey diagram showing the distribution of ferroptosis molecular patterns and ferroptosis gene clusters. B. The differences in distribution of ferroptosis scores among the three ferroptosis-related molecular patterns. C. Differences in distribution of ferroptosis scores among the three ferroptosis gene clusters. D. Survival outcomes between high- and low-risk groups.

Furthermore, we found that the infiltration of immunosuppressive cells, including TAMs, Tregs, and MDSCs, was higher in molecular pattern C compared with molecular pattern A or B. Previous studies demonstrated that TAMs, Tregs, and MDSCs, as the main components in the TME, can enhance HCC proliferation, migration, and immune escape through forming immune suppressive microenvironment [20-23]. For example, TAM can induce angiogenesis by producing angiogenic factors and attract Tregs to infiltrate the TME to inhibit the activity of cytotoxic T cells [24, 25]. In addition, previous studies have demonstrated that Tregs infiltrating the HCC microenvironment are asso-

ciated with poor prognosis [26, 27]. Further, Zhou et al. confirmed that tumor-associated neutrophils (TANs) attract Tregs to infiltrate the HCC microenvironment by secreting CCL17, which promoted the progression of HCC, angiogenesis, and resistance to sorafenib [28]. Regarding MDSCs, Hoechst et al. found that MDSCs inhibited autologous natural killer cells (NK cells), further facilitating the suppression of the immune response [29]. Xu et al. further demonstrated that activated hepatic stellate cells (HSCs) recruited the MDSCs into the HCC microenvironment via SDF/CXCR4 axis, promoting HCC progression and immune evasion [30]. These results suggest that increased infil-
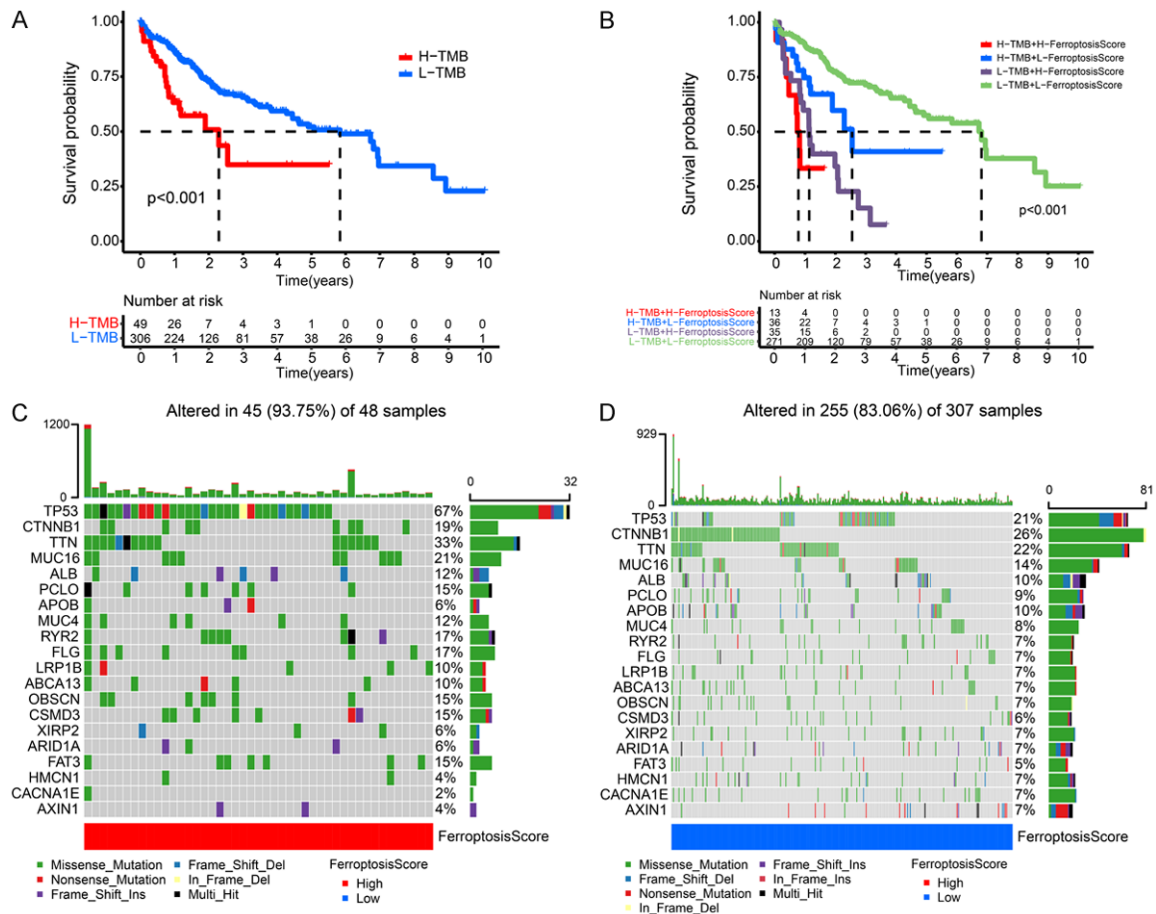
Figure 8. Correlation between ferroptosis score and tumor mutation burden (TMB). (A) Survival outcomes between high- and low-TMB groups. (B) Kaplan-Meier survival curves comparing survival differences for HCC patients grouped by tumor mutation burden and ferroptosis score. (C, D) Mutation frequency differences between high- (C) and low-risk (D) groups.

tration of immunosuppressive cells in the HCC microenvironment is related to poor prognosis. In addition, our molecular patterns based on FRGs can better reflect the biological status of the HCC microenvironment.

Further analyses revealed that expression levels of immune checkpoint molecules were higher in high-risk group than in low-risk group. This was consistent with previous findings that PD-1 and CTLA-4 promoted the tumor immune evasion by negatively mediating T-cell immune function [31]. Furthermore, PD-1 and CTLA-4 are thought to affect T cell-mediated immune response at different stages. CTLA-4 regulates T cell-mediated immune response primarily in lymph nodes in the early phase, whereas PD-1 negatively regulates T cell-mediated immune response mainly in peripheral tissues in the later phase [31, 32]. Shi et al. found that upreg-

ulated peripheral and intratumoral PD-1 expression promoted CD8+ T cells apoptosis. They suggested that PD-1 can serve as a prognostic indicator for HCC patients after surgical resections [33]. For CTLA-4, Wang et al. found that regulatory T cells inhibited dendritic cells-mediated immune function in a CTLA-4-dependent manner [34]. These results indicated that immune checkpoint molecules can be used as prognostic indicators in HCC patients and are potential targets for improving the efficacy of immunotherapy.

In summary, this study reveals how FRGs affect the prognosis of HCC patients. The developed ferroptosis score showed good performance in predicting the survival and assessing the biological status of HCC. However, this study has some limitations. First, this was a retrospective analysis; hence the results should
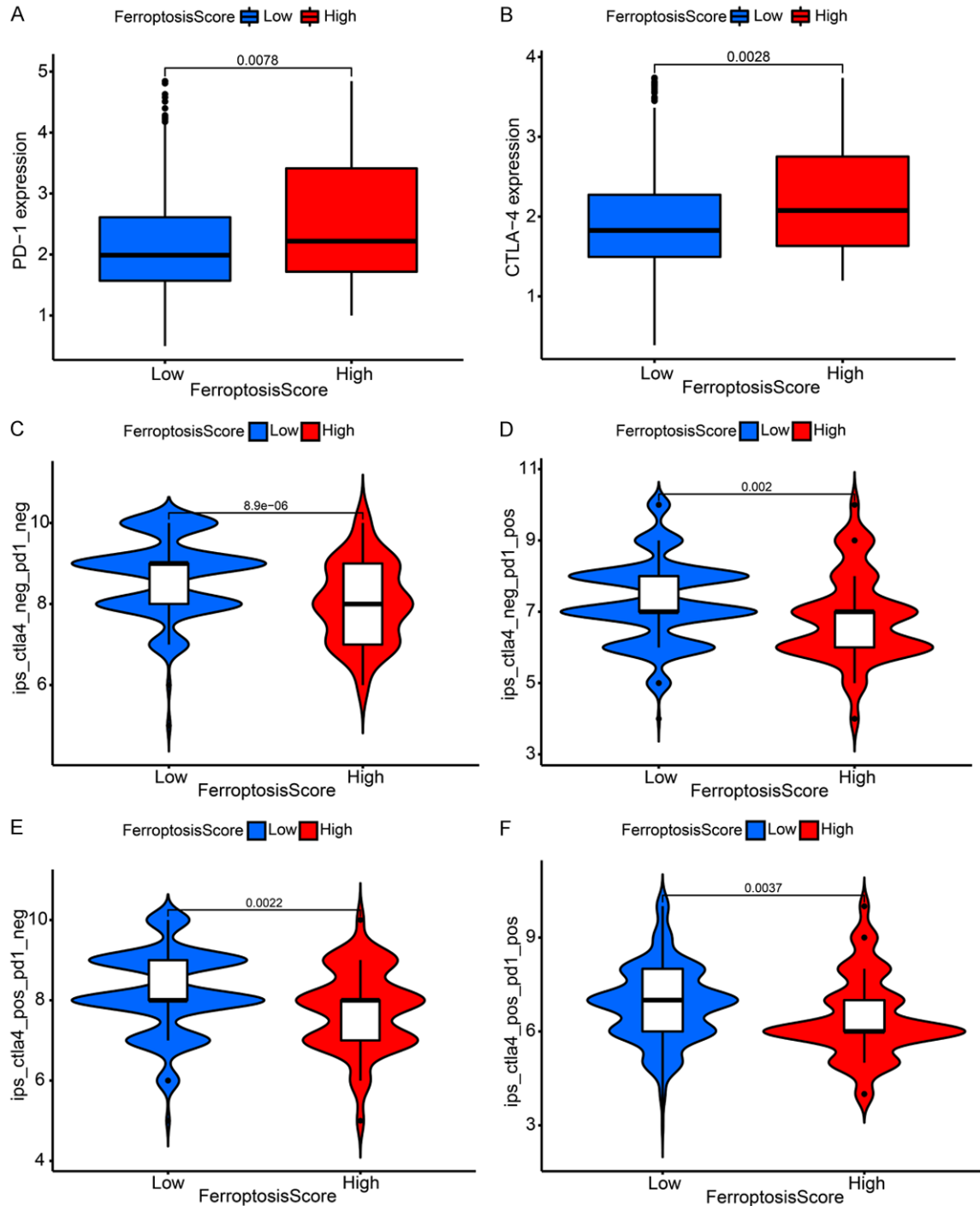
Figure 9. Association between ferroptosis score and response to immunotherapy. (A, B) Expression levels of PD-1 (A) and CTLA-4 (B) were higher in the high-risk group than in the low-risk group. (C-F) Immunotherapy scores were higher in the low-risk group than in the high-risk group.

be validated in prospective studies. Second, the mechanism by which FRGs affect the progression of HCC was not uncovered. Therefore, it should be further investigated through well-designed experiments.

Conclusion

In conclusion, this study demonstrates that FRGs participates in the pathogenesis and progression of HCC. Moreover, ferroptosis-related
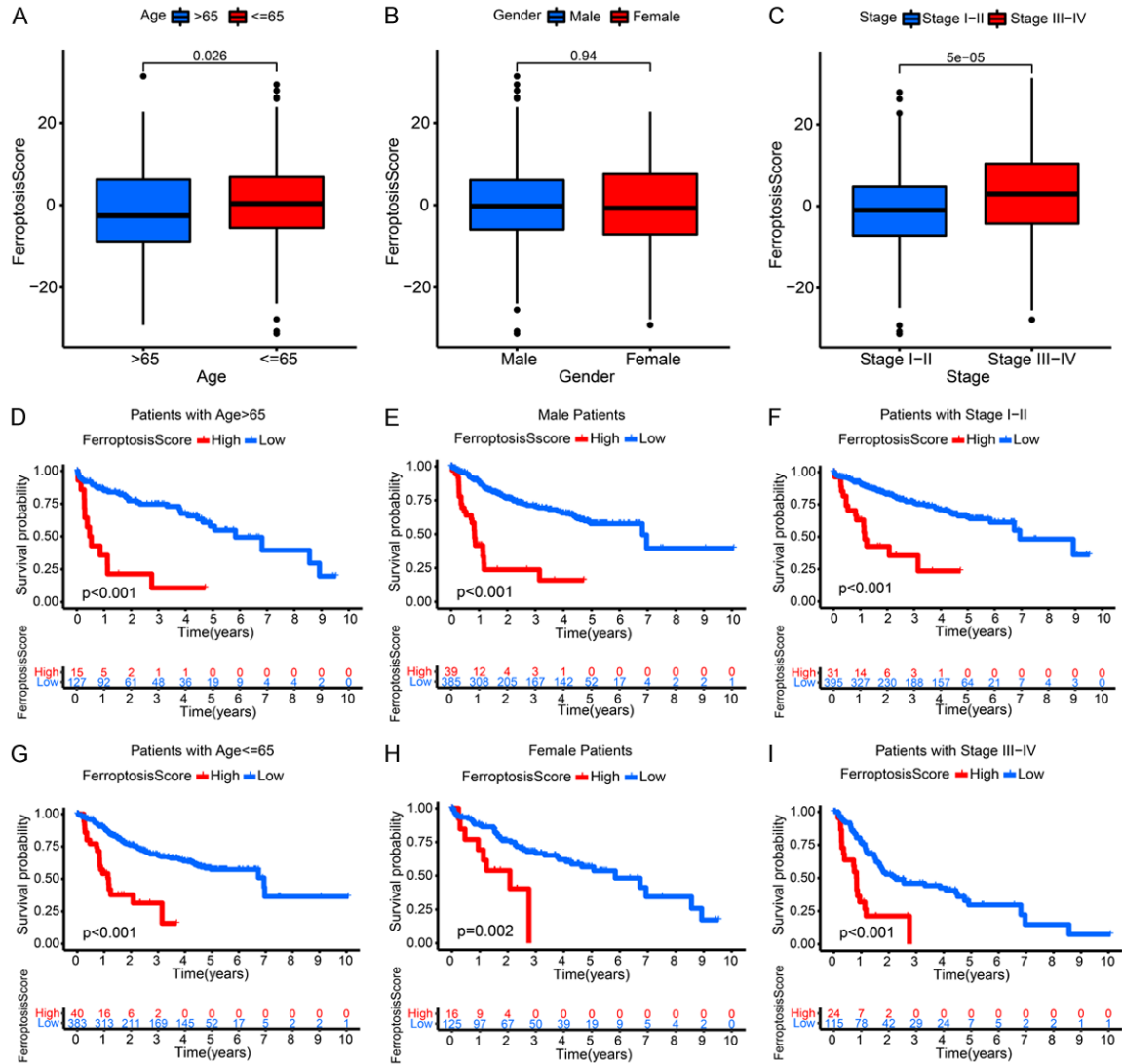
Figure 10. Impact of ferroptosis score on prognosis of HCC patients. (A-C) Box plots showing the difference in distribution of ferroptosis score across clinicopathological features: Age (A), Gender (B), and Stage (C). (D-I) Survival analysis from various patient subgroups including Age >65 (D), Male (E), Stage I-II (F), Age ≤65 (G), Female (H), and Stage III-IV (I).

molecular patterns may influence disease progression and survival outcomes of individual patients by inducing changes in the TME. Importantly, ferroptosis-related molecular patterns can not only help to predict the survival of patients but also provide new perspectives for application of immunotherapy.

Acknowledgements

Disclosure of conflict of interest

None.

Address correspondence to: Tao Luo, General Surgery, Xuanwu Hospital, Capital Medical University, No. 45, Changchun Street, Xicheng District, Beijing, China. E-mail: TaoLuo35@126.com

References

[1] Torre LA, Bray F, Siegel RL, Ferlay J, Lortet-Tieulent J and Jemal A. Global cancer statistics, 2012. CA Cancer J Clin 2015; 65: 87-108.

[2] Bray F, Ferlay J, Soerjomataram I, Siegel RL, Torre LA and Jemal A. Global cancer statistics 2018: GLOBOCAN estimates of incidence and mortality worldwide for 36 cancers in 185 countries. CA Cancer J Clin 2018; 68: 394-424.

[3] Ogunwobi OO, Harricharran T, Huaman J, Galuza A, Odumuwagun O, Tan Y, Ma GX and Nguyen MT. Mechanisms of hepatocellular carcinoma progression. World J Gastroenterol 2019; 25: 2279-2293.

[4] Xu Q, Shi W, Lv P, Meng W, Mao G, Gong C, Chen Y, Wei Y, He X, Zhao J, Han H, Sun M and Xiao K. Critical role of caveolin-1 in aflatoxin B1-induced hepatotoxicity via the regulation of oxidation and autophagy. Cell Death Dis 2020; 11: 6.

[5] Ren YD, Ye ZS, Yang LZ, Jin LX, Wei WJ, Deng YY, Chen XX, Xiao CX, Yu XF, Xu HZ, Xu LZ, Tang YN, Zhou F, Wang XL, Chen MY, Chen LG, Hong MZ, Ren JL and Pan JS. Fecal microbiota transplantation induces hepatitis B virus e-antigen (HBeAg) clearance in patients with positive HBeAg after long-term antiviral therapy. Hepatology 2017; 65: 1765-1768.

[6] Shen Z, Song J, Yung BC, Zhou Z, Wu A and Chen X. Emerging strategies of cancer therapy based on ferroptosis. Adv Mater 2018; 30: e1704007.

[7] Dixon SJ, Lemberg KM, Lamprecht MR, Skouta R, Zaitsev EM, Gleason CE, Patel DN, Bauer AJ, Cantley AM, Yang WS, Morrison B 3rd and Stockwell BR. Ferroptosis: an iron-dependent form of nonapoptotic cell death. Cell 2012; 149: 1060-1072.

[8] Louandre C, Ezzoukhry Z, Godin C, Barbare JC, Maziere JC, Chauffert B and Galmiche A. Iron-dependent cell death of hepatocellular carcinoma cells exposed to sorafenib. Int J Cancer 2013; 133: 1732-1742.

[9] Hirschhorn T and Stockwell BR. The development of the concept of ferroptosis. Free Radic Biol Med 2019; 133: 130-143.

[10] Sun X, Niu X, Chen R, He W, Chen D, Kang R and Tang D. Metallothionein-1G facilitates sorafenib resistance through inhibition of ferroptosis. Hepatology 2016; 64: 488-500.

[11] Liang JY, Wang DS, Lin HC, Chen XX, Yang H, Zheng Y and Li YH. A novel ferroptosis-related gene signature for overall survival prediction in patients with hepatocellular carcinoma. Int J Biol Sci 2020; 16: 2430-2441.

[12] Wang W, Green M, Choi JE, Gijon M, Kennedy PD, Johnson JK, Liao P, Lang X, Kryczek I, Sell A, Xia H, Zhou J, Li G, Li J, Li W, Wei S, Vatan L, Zhang H, Szeliga W, Gu W, Liu R, Lawrence TS, Lamb C, Tanno Y, Cieslik M, Stone E, Georgiou G, Chan TA, Chinnaiyan A and Zou W. CD8(+) T cells regulate tumour ferroptosis during cancer immunotherapy. Nature 2019; 569: 270-274.

[13] Zhang B, Wu Q, Li B, Wang D, Wang L and Zhou YL. m(6)A regulator-mediated methylation modification patterns and tumor microenvironment infiltration characterization in gastric cancer. Mol Cancer 2020; 19: 53.

[14] Chen J and Chloupkova M. Abnormal iron uptake and liver cancer. Cancer Biol Ther 2009; 8: 1699-1708.

[15] Torti SV and Torti FM. Iron and cancer: more ore to be mined. Nat Rev Cancer 2013; 13: 342-355.

[16] Lee S, Mardinoglu A, Zhang C, Lee D and Nielsen J. Dysregulated signaling hubs of liver lipid metabolism reveal hepatocellular carcinoma pathogenesis. Nucleic Acids Res 2016; 44: 5529-5539.

[17] Liu Z, Zhao Q, Zuo ZX, Yuan SQ, Yu K, Zhang Q, Zhang X, Sheng H, Ju HQ, Cheng H, Wang F, Xu RH and Liu ZX. Systematic analysis of the aberrances and functional implications of ferroptosis in cancer. iScience 2020; 23: 101302.

[18] Zhou HZ, Zeng HQ, Yuan D, Ren JH, Cheng ST, Yu HB, Ren F, Wang Q, Qin YP, Huang AL and Chen J. NQO1 potentiates apoptosis evasion and upregulates XIAP via inhibiting proteasome-mediated degradation SIRT6 in hepatocellular carcinoma. Cell Commun Signal 2019; 17: 168.

[19] Yang Y, Zheng J, Wang M, Zhang J, Tian T, Wang Z, Yuan S, Liu L, Zhu P, Gu F, Fu S, Shan Y, Pan Z and Zhou W. NQO1 promotes an aggressive phenotype in hepatocellular carcinoma via amplifying ERK-NRF2 signaling. Cancer Sci 2021; 112: 641-654.

[20] Lu C, Rong D, Zhang B, Zheng W, Wang X, Chen Z and Tang W. Current perspectives on the immunosuppressive tumor microenvironment in hepatocellular carcinoma: challenges and opportunities. Mol Cancer 2019; 18: 130.

[21] Ding T, Xu J, Wang F, Shi M, Zhang Y, Li SP and Zheng L. High tumor-infiltrating macrophage density predicts poor prognosis in patients with primary hepatocellular carcinoma after resection. Hum Pathol 2009; 40: 381-389.

[22] Park H, Jung JH, Jung MK, Shin EC, Ro SW, Park JH, Kim DY, Park JY and Han KH. Effects of transarterial chemoembolization on regulatory T cell and its subpopulations in patients with hepatocellular carcinoma. Hepatol Int 2020; 14: 249-258.

[23] Chiu DK, Tse AP, Xu IM, Di Cui J, Lai RK, Li LL, Koh HY, Tsang FH, Wei LL, Wong CM, Ng IO and Wong CC. Hypoxia inducible factor HIF-1 promotes myeloid-derived suppressor cells accumulation through ENTPD2/CD39L1 in hepatocellular carcinoma. Nat Commun 2017; 8: 517.

[24] Deryugina EI and Quigley JP. Tumor angiogenesis: MMP-mediated induction of intravasation- and metastasis-sustaining neovasculature. Matrix Biol 2015; 44-46: 94-112.

[25] Wang D, Yang L, Yue D, Cao L, Li L, Wang D, Ping Y, Shen Z, Zheng Y, Wang L and Zhang Y. Macrophage-derived CCL22 promotes an immunosuppressive tumor microenvironment via IL-8 in malignant pleural effusion. Cancer Lett 2019; 452: 244-253.

[26] Jiang R, Tang J, Chen Y, Deng L, Ji J, Xie Y, Wang K, Jia W, Chu WM and Sun B. The long noncoding RNA lnc-EGFR stimulates T-regulatory cells differentiation thus promoting hepatocellular carcinoma immune evasion. Nat Commun 2017; 8: 15129.

[27] Yang P, Li QJ, Feng Y, Zhang Y, Markowitz GJ, Ning S, Deng Y, Zhao J, Jiang S, Yuan Y, Wang HY, Cheng SQ, Xie D and Wang XF. TGF-beta-miR-34a-CCL22 signaling-induced Treg cell recruitment promotes venous metastases of HBV-positive hepatocellular carcinoma. Cancer Cell 2012; 22: 291-303.

[28] Zhou SL, Zhou ZJ, Hu ZQ, Huang XW, Wang Z, Chen EB, Fan J, Cao Y, Dai Z and Zhou J. Tumor-associated neutrophils recruit macrophages and T-regulatory cells to promote progression of hepatocellular carcinoma and resistance to sorafenib. Gastroenterology 2016; 150: 1646-1658, e1617.

[29] Hoechst B, Voigtlaender T, Ormandy L, Gamrekelashvili J, Zhao F, Wedemeyer H, Lehner F, Manns MP, Greten TF and Korangy F. Myeloid derived suppressor cells inhibit natural killer cells in patients with hepatocellular carcinoma via the NKp30 receptor. Hepatology 2009; 50: 799-807.

[30] Xu Y, Fang F, Jiao H, Zheng X, Huang L, Yi X and Zhao W. Activated hepatic stellate cells regulate MDSC migration through the SDF-1/CXCR4 axis in an orthotopic mouse model of hepatocellular carcinoma. Cancer Immunol Immunother 2019; 68: 1959-1969.

[31] Buchbinder EI and Desai A. CTLA-4 and PD-1 pathways: similarities, differences, and implications of their inhibition. Am J Clin Oncol 2016; 39: 98-106.

[32] Xu F, Jin T, Zhu Y and Dai C. Immune checkpoint therapy in liver cancer. J Exp Clin Cancer Res 2018; 37: 110.

[33] Shi F, Shi M, Zeng Z, Qi RZ, Liu ZW, Zhang JY, Yang YP, Tien P and Wang FS. PD-1 and PD-L1 upregulation promotes CD8(+) T-cell apoptosis and postoperative recurrence in hepatocellular carcinoma patients. Int J Cancer 2011; 128: 887-896.

[34] Chen X, Du Y, Hu Q and Huang Z. Tumor-derived CD4+CD25+regulatory T cells inhibit dendritic cells function by CTLA-4. Pathol Res Pract 2017; 213: 245-249.